Optics Communications 475 (2020) 126264

Contents lists available at ScienceDirect

Optics Communications

journal homepage: www.elsevier.com/locate/optcom

A long wavelength infrared narrow-band reflection filter based on an asymmetric hexagonal structure

Yuhao Zhang [a,b], Zhongzhu Liang [a,*], Dejia Meng [a], Xiaoyan Shi [a,b], Zheng Qin [a,b], Fuming Yang [a,b], Lichao Zhang [a], Yuxin Qin [a], Jinguang Lv [a], Xiaoyi Wang [a], Xingyu Xu [a,c], Haihong Yu [a,c]

[a] State Key Laboratory of Applied Optics, Changchun Institute of Optics, Fine Mechanics and Physics, Chinese Academy of Sciences, Changchun, Jilin, 130033, China

[b] University of the Chinese Academy of Sciences, China

[c] Key Lab of Coherent Light, Atomic and Molecular Spectroscopy, Ministry of Education; College of Physics, Jilin University, Changchun 130012, China

ARTICLE INFO

Keywords:
Narrow-band filter
Long wavelength infrared
Dielectric material

ABSTRACT

An asymmetric hexagon structure is designed on the micrometer scale to fabricate a narrow-band reflection filter in the long wavelength infrared band. By rotating the hexagon structure 20 degrees, a single narrow-band resonance can be achieved at 7.99 μm with high reflectivity of 92% and Q value of 200 simultaneously. The spectral resolution is 40 nm, and the average reflectivity exceeds 90%. By changing the size of the unit cell through a scaling factor k, it can filter across 8-12 μm (25 THz–37.5 THz). The dephasing time of the proposed filter is 1.7 ps. We also studied the filtering properties of the proposed filter with significant figure of merit and insertion losses. The average figure of merit can reach 300, and the insignificant insertion loss is only 0.4 dB. The subwavelength filter structure consists of a periodic array of dielectric substrates made of BaF_2 and hexagon structure made of Ge with low intrinsic loss, which requires very few layers compared to traditional filters with multilayer films. In addition, the proposed structure is independent to the angles of the incident light. Moreover, it possesses a good tolerance of rounding issue in micro-fabrication process. The position of the center wavelength of the spectra has hardly shift when the sharp vertices become round. The structure can be applied in biosensor and hyperspectral imaging systems.

1. Introduction

Long wavelength infrared (LWIR) radiation mainly comes from the self-heating radiation of a normal-temperature object or molecular chemical bond vibration. Narrow-band filters working in LWIR can be used in biological sensing [1]. In addition, it can also be applied in hyperspectral imaging systems to achieve high-sensitivity, high-resolution hyperspectral imaging detection under certain circumstances such as clutter zone targets and high background interference.

Traditionally, a narrow-band filter consists of dozens layers thin-films even more than 100 layers with different thickness of each layer [2]. Multiple reflections and transmissions on the interface of each film are used to achieve optical interference and linear superposition so that the in-phase components of the transmitted light intensify and the reverse-phase components cancel. Therefore, to obtain a filter with good performance, it is necessary to design a multilayer film system and the thickness of each film is different. Failure to control the thickness of any layer of these films will cause the failure of the traditional multiple thin-films narrow-band filter. Thus, when operating in the LWIR is required, traditional filters suffer from fabrication difficulties and complexities due to dozens or more of layered thick films [3].

In recent years, narrow-band filters working in the LWIR and analogous devices have been possible to use the surface resonance modes of subwavelength structures based on guided mode resonance (GMR) [4–8] and surface plasmon resonance (SPR) [9–12]. Filters based on subwavelength structures consist of less layers have the advantage of thin thickness and low material cost, unlike thin-film filters. However, there are usually multiple transmission or reflection peaks in a wide spectral range when utilizing GMR and SPR with metal. In addition, due to the strong absorption of light in the metal, filters utilizing SPR are usually accompanied by a wide spectral linewidth, which is detrimental to narrowband filtering. Recently, SPR such as Fano resonance using metal or dielectric materials [13–15], electromagnetically induced transparency (EIT) [16] and epsilon-near-zero (ENZ) modes [17] can realize narrow-band reflection or transmission detection but they usually work in the THz band or mid-wave infrared band other than LWIR. In addition, the reflectivity or transmission are below 80%.

* Corresponding author.
E-mail address: liangzz@ciomp.ac.cn (Z. Liang).

https://doi.org/10.1016/j.optcom.2020.126264
Received 15 April 2020; Received in revised form 2 July 2020; Accepted 11 July 2020
Available online 13 July 2020
0030-4018/

In order to solve the above problems, metasurfaces based on a high-refractive-index dielectric material becomes the better choice because of the low intrinsic loss and unique ability of controlling the propagation and localization of light in LWIR.

A new hexagonal dielectric subwavelength structure is proposed in this paper for narrow-band optical reflection filters working in the LWIR. A two-layer structure of Ge-BaF_2 is designed on the micrometer scale. It is thinner because two layers are required thus the process is simplified. High reflectivity and high Q value can be achieved at the same time in our proposed design. It shows additional advantages of being independent to the angles of incident light. Based on changing the scaling ratio k of the unit cell, a single high-Q resonance can be obtained across the LWIR (8-12 μm) which makes the design of the long wavelength infrared narrow-band filters possible.

2. Structure design and methods

The theory of bound states in the continuum (BICs) was first proposed in quantum mechanics. In 1929, von Neumann and Wigner showed that Schrödinger's equation can have bound states above the continuum threshold that manifest themselves as resonances that do not decay [18]. A true BIC is a mathematical object with an infinite Q value and a vanishing resonance width, and it can exist only in ideal lossless infinite structures or for extreme parameter values [19–21]. Recently, it has been recognized that a BIC is essentially a wave phenomenon and therefore is not limited to the field of quantum mechanics. BICs have been shown to occur in many different areas of wave physics, including acoustics, microwaves, and nanophotonics. By using a cavity that supports multiple standing waves, the structure of the cavity can be tuned until the system most closely meets the conditions required for a BIC in the corresponding infinite system. At this point, a BIC can be realized as a quasi-BIC, which is also known as a supercavity mode [22]. Although the Q value and resonance width are limited [23,24], a high-Q quasi-BIC can still be achieved in photonic crystal plates [20,22,25,26], coupled optical waveguides [27–30] and even isolated dielectric particles [31].

The realization of a quasi-BIC relies on the distortion of the symmetry-protected bound state in the continuum. That is, when the in-plane reverse symmetry of the unit cell is destroyed, a true BIC is transformed into a quasi-BIC. At this time, the magnitude of the Q value is related to the material, structure and asymmetry parameters of the unit cell and can be expressed as [32]:

$$Q = Q_0 \alpha^{-2} \tag{1}$$

Here, α is an asymmetry parameter that has different meanings for different structures, but its value is between 0 and 1. The value of Q_0 is determined by the design of the metasurface, being independent on α [32].

In this paper, we design a two-layer periodic structure on the micrometer scale shown in Fig. 1. The in-plane reverse symmetry of the unit cell is destroyed by rotating the structure. The asymmetry parameter here is the angle β between the y axis and the long axis of the hexagon. The ideal structure supports a symmetry-protected BIC [33] at β=0°. By breaking the in-plane inversion symmetry (x, y)→(-x, -y), it transforms into a quasi-BIC, achieving a high-Q reflection peak at 7.99 μm.

In the two-layer structure, the bottom layer is a BaF_2 substrate (due to the transmittance of BaF_2 is 90% in the LWIR and its loss is small), and the refractive index of BaF_2 is n'=1.43. The material of the hexagonal structure is Ge (due to its high refractive index(real part) in the LWIR, low extinction coefficient and cost), and k is the scaling ratio of the unit cell. As shown in Fig. 1, X and Y are the length and width parameters of the periodic structure respectively, where X=5.6 μm and Y=3.2 μm. A and B are the length parameters of the hexagonal structure, where A=2.8 μm and B=1.3 μm. The value of h, the thickness of the hexagon, is set to 0.7 μm. β is the angle between the long axis of the hexagonal structure and the y axis, and the value is set to 20 degrees. β is the parameter that destroys the inversion symmetry of the structure, and its relationship with the asymmetry parameter α in this structure is:

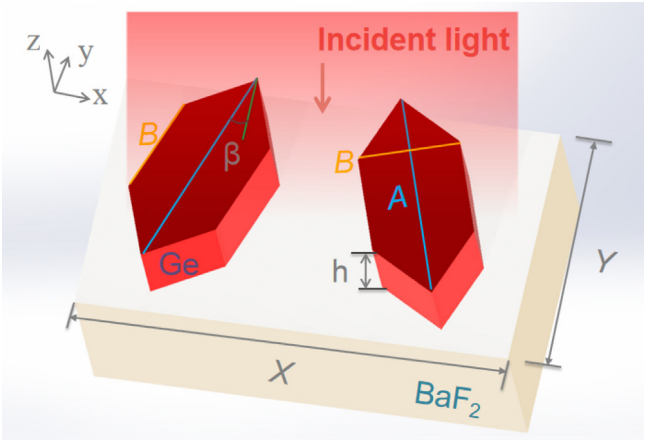

Fig. 1. Schematic diagram of the proposed LWIR reflection filter. The structure consists of a periodic array of dielectric substrates made of BaF_2 and hexagon structure made of Ge. X and Y are the length and width parameters of the periodic structure respectively, where X=5.6 μm and Y=3.2 μm. A and B are the length parameters of the hexagonal structure, where A=2.8 μm and B=1.3 μm. The value of h, the thickness of the hexagon, is set to 0.7 μm. β is the angle between the long axis of the hexagonal structure and the y axis, and $\beta = 20$ degrees.

$$\alpha = \sin(\beta) \tag{2}$$

According to Eq. (1), the Q value of the reflection peak designed in this paper is:

$$Q = Q_0[\sin(\beta)]^{-2} \tag{3}$$

Here, the value of Q_0 is determined by the design of the structure, regardless of α [32]. According to Eq. (3), although there are many factors affecting the Q value, the main influencing factor is the asymmetric parameter, which even causes the Q value to be different in magnitude.

The finite-difference time-domain method (FDTD) is widely used in optical calculations. And FDTD method was used to simulate the continuous array of BIC-based structures proposed in this paper. Perfectly matched layer (PML) boundaries were employed along the beam propagation direction (z-axis) and periodic boundaries were employed for the x and y axes. The unit cell geometry was approximated using a tetrahedral mesh and a plane-wave pulse served as a long wavelength infrared source. The dielectric function of simulated Ge was taken from the empirically defined values by Palik [34].

3. Results and discussion

Fig. 2(a) shows the reflection spectra of the designed structure under the normal incidence and an enlarged view of the resonance. According to Fig. 2(a), the reflectivity can reach 92% at 7.99 μm (which means the characteristic frequency of the filter we proposed is 37.5 THz) with a full-width at half-maximum (FWHM) of 40 nm, while the reflectivity at other wavelengths in the range of 7.5–12 μm is maintained at approximately 10%. In addition, the Q value of the reflection peak is as high as 200. These results suggest that the proposed structure can be used as a narrow-band reflection filter working in the LWIR. The electric field distribution of the structure at 7.99 μm is shown in Fig. 2(b).

The supercavity resonance [22] caused by the Ge structure results in the formation of a "trapped mode" [35] weakly coupled to free space due to the symmetry of the dielectric structure. In Fig. 2(b), it can be observed that the electric field is concentrated at the sharp vertices of

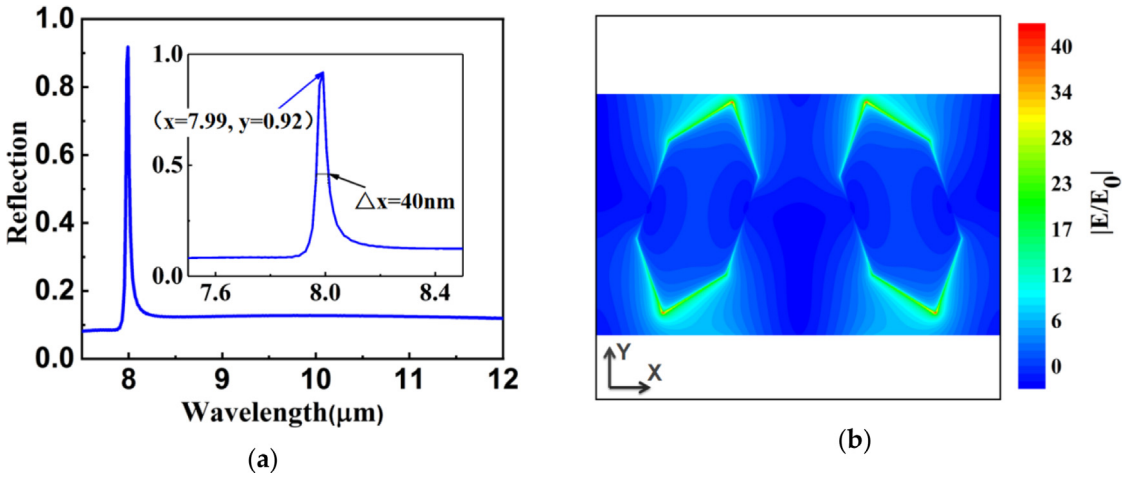

Fig. 2. (a) The reflection spectra of the filter at normal incidence. Inset shows enlarged view of the resonance. (b) The electric field distribution of the structure at 7.99 μm.

the hexagons and reached a larger amplification of the near field [36] compared to the structure without sharp vertices such as ellipse. So we choose hexagon to design not ellipse or others.

Fig. 3(a) shows the simulated reflection spectra and related Q value obtained by changing the length of A without changing B to get the proper A/B parameters of hexagon. It can be seen from the red dotted line in Fig. 3 that as A/B increases, the Q value decrease from 381 to 119. Moreover, the reflectivity of the resonance gradually increases, which can reach up to 98%, and the position of the resonance has a redshift. In order to meet the requirements of high reflectivity and high Q of the filter in this paper, B = 2.8 μm is selected as the parameter of hexagon. Fig. 3(b) illustrate the dephasing time and the figure of merit (FoM) of the resonance as a function of A. Microscopically, the dephasing time is controlled by coupling of the resonance to the electron–hole pair continuum, and by radiation damping, which is important in large particles above a radius of ca. 10 nm [37]. It is a critical parameter that can be defined by taking to account of the resonance narrowness as following [38]:

$$T = 2\hbar/\delta \tag{4}$$

Here, $\hbar$ is the reduced Planck's constant and δ is the homogeneous linewidth of the resonance. For the resonance at 7.99 μm (37.5 THz), the dephasing time is estimated as 1.7 ps. FoM is an important indicator of the filtering properties of the notch filters. It is given by,

$$FoM = \omega 0/\Delta\omega \tag{5}$$

where ω_0 is the center frequency of the resonance and $\Delta\omega$ is the 3 dB bandwidth of the resonance. According to Fig. 3(b), both dephasing time and FoM decreased with increasing A.

According to BIC theory, the quasi-BIC mode caused by the asymmetry of the unit cell is the key to achieving the high Q value of the resonance. The asymmetry of the dielectric structure proposed in this paper is caused by the rotation angle of the hexagonal structure. Moreover, according to Eq. (2), changing the rotation angle will greatly change the magnitude of the Q value. Fig. 4(a) shows the simulated reflection spectra for different rotation angles and their relationship with the Q value. We only change the rotation angle β and keep other parameters unchanged. The vertical placement of the hexagonal structure is defined as a rotation angle of zero. The hexagons are simultaneously rotated clockwise and counterclockwise by the same angle. The angle varies from 2.5 to 45 degrees. As shown in the red dotted line diagram in Fig. 4(a), the Q value of the resonance exhibits a decreasing trend with an increase in the angle of rotation, and the trend of the change approximates the shape of a hyperbola. When the rotation angle is 2.5 degrees, the Q value is as high as 1370; when the angle is 5 degrees, the Q value of the reflection peak decreases to 412. As β selects the maximum rotation angle of 45 degrees, the Q value is only 62. The change of β produced an order of magnitude change in the Q value. These trends are consistent with Eq. (2). Fig. 4(b) illustrate the dephasing time and FoM as a function of β. Although Q value and FoM is higher for a smaller angle, the small angle also causes the reflectivity to decrease rapidly. Considering the influence of the rotation angle on these parameters, we choose 20 degrees as the angle parameter for the filter design.

The simulated reflection spectra obtained by changing the material of the hexagon (changing the refractive index of the material) is shown in Fig. 5(a). As the refractive index of the material increases, the Q value of the resonance fluctuates around 240, increasing and decreasing with different amplitudes. In addition, the position of the resonance produces significant redshift and the reflectivity also increases with increasing refractive index. The related FoM is shown in Fig. 5(b). Although the FoM is decreased as the index increased, it still remained above 300. To design a narrow-band reflection filter working in LWIR with high reflectivity and high Q value, the refractive index should be as high as possible according to Fig. 5. The refractive index of Ge is up to 4 in the LWIR(and low extinction coefficient and cost), which makes it the best choice in this paper.

The reflection filter we proposed can reject light at any certain wavelength between 8-12 μm (25 THz–37.5 THz). The position of the resonance is determined by the scaling factor k. We will discuss the effect of k on resonance, the angle-independent performance in the next part and the rounding issue of the sharp vertices contained in the hexagon structure inherent in micro-fabrication process.

3.1. The scaling factor k

In this paper, k is defined as a scaling factor to scale the unit cell designed. When k takes a certain value, the value of A, B, X, Y will take the value in Fig. 1 and multiply by k. The filter we proposed can effectively work at 7.99 μm. By modulating k, the range of the proposed reflection filter could effectively cover a wide range of operation wavelengths, from 8 μm to 12 μm (25 THz to 37.5 THz). Fig. 6(a) shows the simulated reflection spectra for the scaling range of 1–1.55. It can be found that the scaling of the unit cell can enable an adjustment of the position of the resonance. As k increases, the peak position of the resonance is redshifted. In addition, the scaling factor exhibits a linear relationship with the peak position of the resonance, which can be seen from the blue curve in Fig. 6(b). The red curve in Fig. 6(b) shows the relationship between the Q value and the scaling factor k. With the change in k from 1 to 1.55, the Q value is fluctuating up and down near 190, and the change is relatively stable. This is consistent with the influence of the Q value mentioned above; that is,

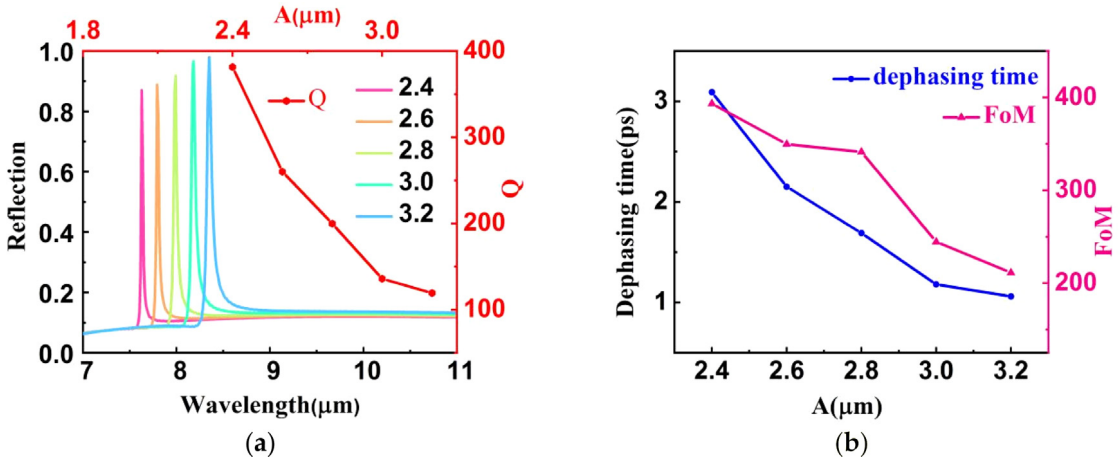

Fig. 3. (a) The reflection spectra and associated Q values as A changes. (b) The dephasing time and FoM of the resonance as a function of A.

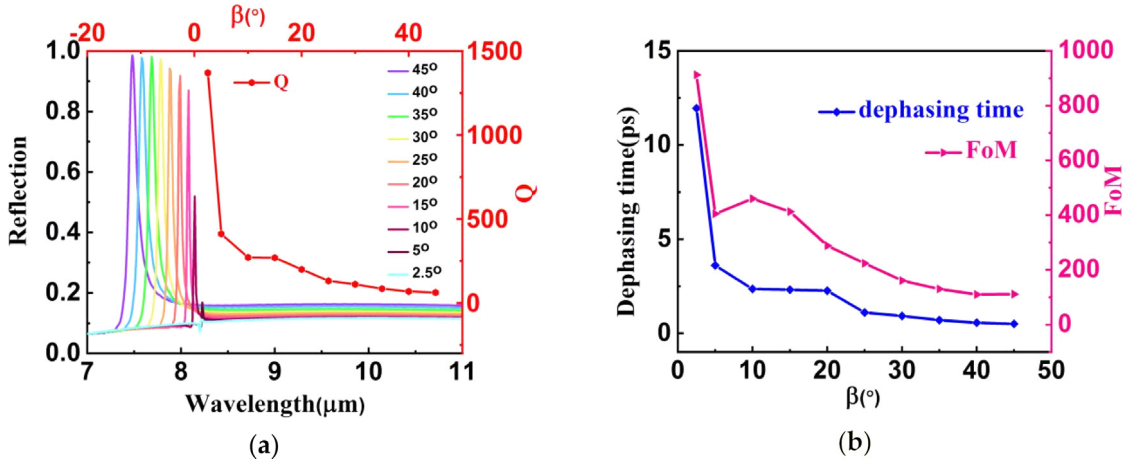

Fig. 4. (a) The reflection spectra and associated Q values as the angle of rotation β changes. (b) The dephasing time and FoM of the resonance as a function of β.

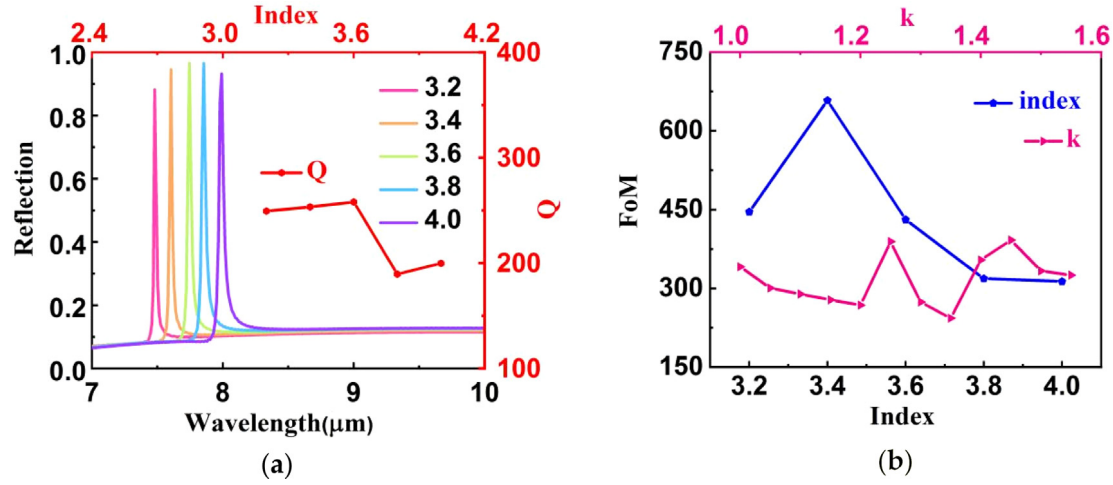

Fig. 5. (a) The reflection spectra and associated Q values as the index of dielectric material changes. (b) The FoM of the resonance as a function of index and k respectively.

the main influencing factor of the Q value is the asymmetry parameter, so the magnitude of the Q value does not vary appreciably.

In addition, we also calculated the insertion loss of the proposed filter. In optical systems, insertion loss can be defined [39,40] as $IL(\mathrm{dB}) = -10\log 10(|T_{\max}|)$, where $T_{\max}$ is the transmittance at peak position. Thus the insertion loss for the proposed filter can be determined as ~0.4 dB, which is negligible.

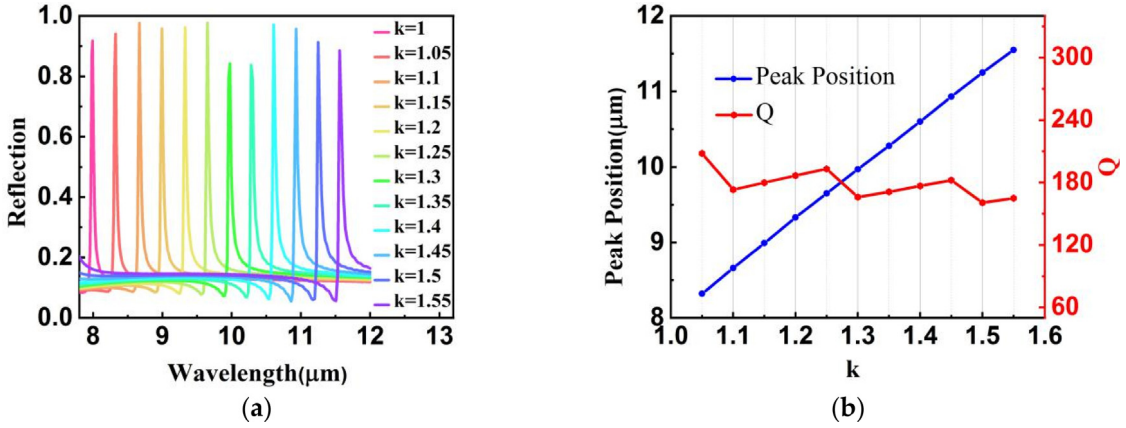

Fig. 6. (a) Comparison of the reflection spectra obtained by changing the scaling ratio k. (b) Peak position and relating Q values obtained by changing k . (For interpretation of the references to color in this figure legend, the reader is referred to the web version of this article.)

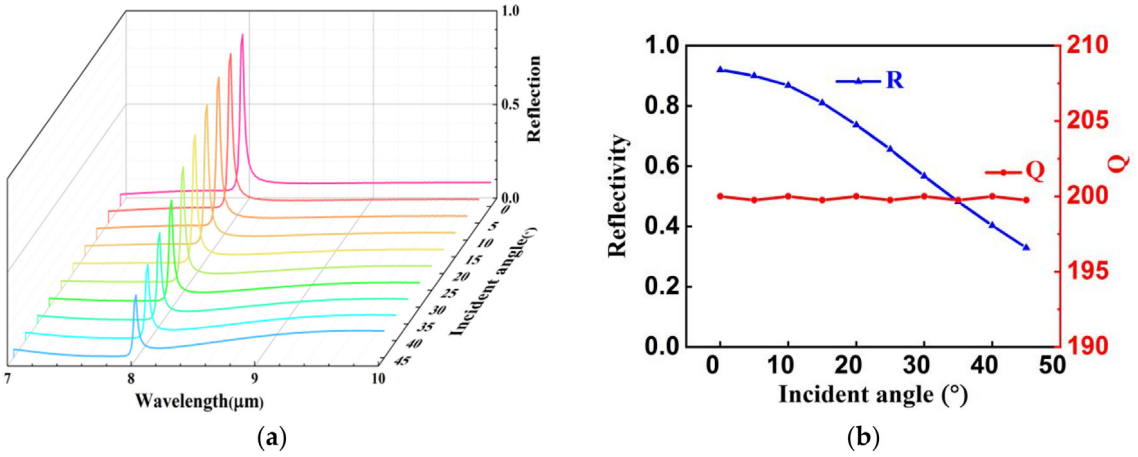

Fig. 7. (a) The reflection spectra as the angle of incidence changes from 0 to 45 degrees. (b) The reflectivity and relating Q values obtained by changing incident angle.

3.2. The angle-independent performance

In most filter designs, angle-independent performance is paramount. Therefore, we simulate the effect of angle of incidence on the device's performance. The angle at normal incidence is defined as 0°. Although, the reflectivity has decreased with the increasing angle according to Fig. 7(b), it can be seen from Fig. 7(a) that the center wavelength of the spectra has hardly shift during the angle of incidence changes from 0° to 45°. In addition, the Q value remains almost unchanged at 200. The filter proposed in this paper can accurately reflect light at any expected wavelength even the angle of incidence is greatly deviated. Therefore, the proposed filter is independent to angles of incident light.

3.3. Rounding issue in micro-fabrication process

The hexagon structure proposed in this paper contains several sharp vertices. Due to these sharp vertices, the near-field magnification is reached [36]. But it is difficult to experimentally realize due to rounding issues inherent in micro-fabrication process. As shown in Fig. 8, these sharp vertices will be rounded in the experiment, so we also simulated this situation. Inset shows an enlarged view at rounded corners and R is the radius parameter of the arc.

The simulated reflection spectra is shown in Fig. 9(a), as can be seen, when R < 0.1 μm, the position of the center wavelength of the spectra has hardly shift. As R continues to increase, a slight blueshift occurs in the center wavelength of the spectra. The reflectivity and relating Q values both decrease when R increases according to Fig. 9(b). However in a micro-fabrication process in real-world, it is possible to achieve R < 0.1 μm. So the filter we proposed is not required to change in experimental realization.

4. Conclusions

In this paper, a long wavelength infrared reflective narrow-band optical filter is designed based on asymmetric hexagons structure made of dielectric material. We numerically demonstrate that, by changing the scaling ratio k of the unit cell, the range of the proposed filter could effectively cover a wide range of operation wavelengths, from 8 μm to 12 μm (25 THz–37.5 THz), with the reflectivity reaching above 90%. And k exhibits a linear relationship with the position of the center wavelength of the resonance. The subwavelength filter structure we proposed consists of a periodic array of dielectric substrates made of BaF_2 and the hexagon structure made of Ge. Because of the low intrinsic loss of Ge, a single resonance with high reflectivity and high Q value can be achieved at 7.99 μm. The Q value reached 200 and the reflectivity achieved 92% at the same time. Moreover, it is verified that the value of Q factor of the resonance is mainly affected by the asymmetry parameter, and the range of influence can reach orders of magnitude. By changing the asymmetry parameter, the maximum Q value can reach 1370. And the dephasing time of the proposed filter is 1.7 ps. We also studied the filtering properties of the proposed filter with significant FoM and insertion losses. The average FoM of the proposed filter can reach 300, and the insignificant insertion loss is only 0.4 dB. In addition, it is proved through simulation that the proposed

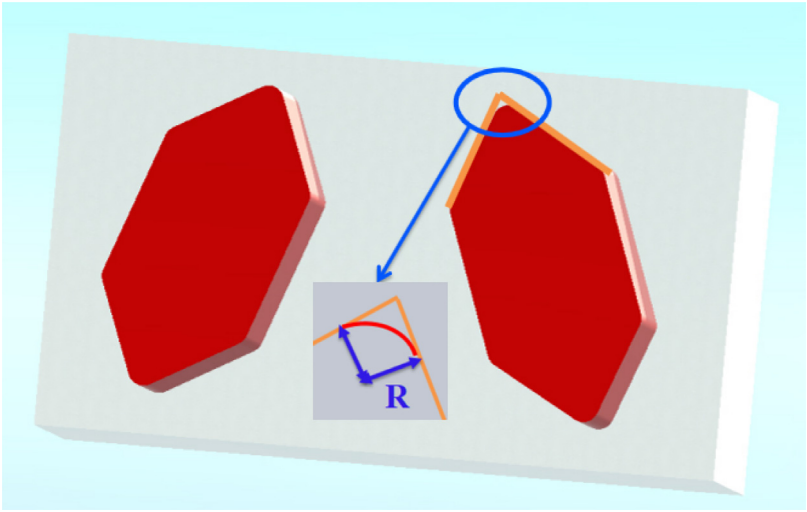

Fig. 8. Schematic diagram of the proposed device under experimental constraints. Inset shows enlarged diagram at rounded corners. R is the radius parameter of the arc.

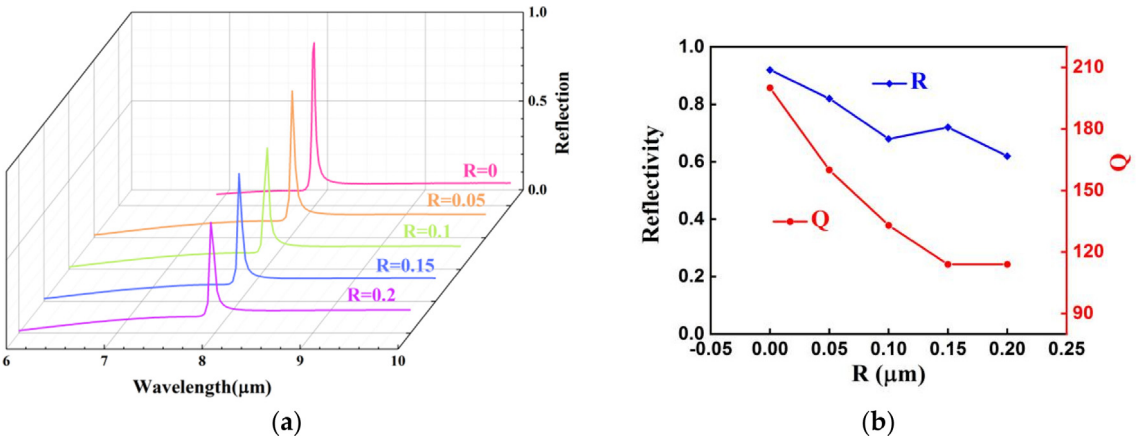

Fig. 9. (a) The reflection spectra when the sharp vertices is rounded in the experiment. (b) The reflectivity and relating Q values when sharp vertices become rounded in the experiment.

filter is independent to angles of incident light. As the angle of the incident light changes from 0 degree to 45 degrees, the position of the center wavelength of the resonance hardly changes. The filter we proposed can also be used in biological sensing and hyperspectral imaging systems to achieve high-sensitivity, high-resolution hyperspectral imaging detection under certain circumstances, providing a reference for designing similar functional devices.

CRediT authorship contribution statement

Yuhao Zhang: Writing - original draft. **Zhongzhu Liang:** Writing - review & editing. **Dejia Meng:** Methodology. **Xiaoyan Shi:** Data curation. **Zheng Qin:** Validation. **Fuming Yang:** Resources. **Lichao Zhang:** Supervision. **Yuxin Qin:** Visualization. **Jinguang Lv:** Methodology. **Xiaoyi Wang:** Supervision. **Xingyu Xu:** Investgation. **Haihong Yu:** Software.

Declaration of competing interest

The authors declare that they have no known competing financial interests or personal relationships that could have appeared to influence the work reported in this paper.

Acknowledgments

This research was funded by the National Natural Science Foundation of China (NSFC) (61735018, 61376122 and 61805242), Scientific and Technological Development Project of Jilin province (20170204077GX, 20190103014JH), Excellent Member of Youth Innovation Promotion Association CAS (2014193, Y201836), Leading Talents and Team Project of Scientific and Technological Innovation for Young and Middle-aged Groups in Jilin Province (20190101012JH), Overseas Students Science and Technology Innovation and Entrepreneurship Projects, Project of CIOMP-Duke Collaborative Research (201203002), Project of CIOMP-Fudan University Collaborative Research and Independent fund of State Kay Laboratory of Applied Optics, CAS President's International Fellowship Initiative (PIFI).

References

[1] Andreas Tittl, Aleksandrs Leitis, Mingkai Liu, Imaging-based molecular barcoding with pixelated dielectric metasurfaces, Science 360 (2018) 1105–1109, http://dx.doi.org/10.1126/science.aas9768.

[2] M. Vignaux, F. Lemarchand, C. Grezes-Besset, J. Lumeau, In situ optical monitoring of Fabry–Perot multilayer structures: analysis of current techniques and optimized procedures, Opt. Express 25 (15) (2017) 18040–18055, http://dx.doi.org/10.1364/OE.25.018040.

[3] G. Hawkins, R. Sherwood, K. Djotni, Mid-infrared filters for astronomical and remote sensing instrumentation, Proc. SPIE 7101 (2008) 710114, http://dx.doi.org/10.1117/12.796635.

[4] Yunxin Han, Junbo Yang, Xin He, Multiband notch filter based guided-mode resonance for mid-infrared spectroscopy, Opt. Commun. 445 (2019) 64–68, http://dx.doi.org/10.1016/j.optcom.2019.04.018.
[5] T. Kondo, S. Ura, R. Magnusson, Design of guided-mode resonance mirrors for short laser cavities, J. Opt. Soc. Amer. A 32 (8) (2015) 1454–1458, http://dx.doi.org/10.1364/josaa.32.001454.
[6] G. Chen, K.J. Lee, R. Magnusson, Periodic photonic filters: theory and experiment, Opt. Eng. 55 (3) (2016) 037108, http://dx.doi.org/10.1117/1.OE.55.3.037108.
[7] D.W. Peters, R.R. Boye, J.R. Wendt, R.A. Kellogg, S.A. Kemme, T.R. Carter, S. Samora, Demonstration of polarization-independent resonant subwavelength grating filter arrays, Opt. Lett. 35 (19) (2010) 3201–3203, http://dx.doi.org/10.1364/OL.35.003201.
[8] Yanhui Wang, Xiangjun Li, Tingting Lang, Xufeng Jing, Zhi Hong, Multiband guided-mode resonance filter in bilayer asymmetric metallic gratings, Opt. Laser Technol. 103 (2018) 135–141, http://dx.doi.org/10.1016/j.optlastec.2018.01.017.
[9] Binfeng Yun, Guohua Hu, Yiping Cui, Theoretical analysis of a nanoscale plasmonic filter based on a rectangular metal–insulator–metal waveguide, J. Phys. D: Appl. Phys. 43 (2010) 385102, http://dx.doi.org/10.1088/0022-3727/43/38/385102.
[10] L. Duempelmann, A. Luu-Dinh, B. Gallinet, L. Novotny, Four-fold color filter based on plasmonic phase retarder, ACS Photon. 3 (2) (2015) 190–196, http://dx.doi.org/10.1021/acsphotonics.5b00604.
[11] B. Zeng, Y. Gao, F.J. Bartoli, Ultrathin nanostructured metals for highly transmissive plasmonic subtractive color filters, Sci. Rep. 3 (1) (2013) 2840, http://dx.doi.org/10.1038/srep02840.
[12] B. Yun, G. Hu, Y. Cui, Resonant mode analysis of the nanoscale surface plasmon polariton waveguide filter with rectangle cavity, Plasmonics 8 (2) (2013) 267–275, http://dx.doi.org/10.1007/s11468-012-9384-y.
[13] Chen Yan, Kuang-Yu Yang, Olivier J.F. Martin, Fano-resonance-assisted metasurface for color routing, Light: Sci. Appl. 6 (2017) e17017, http://dx.doi.org/10.1038/lsa.2017.17.
[14] Fuli Zhang, XinChao Huang, Qian Zhao, Fano resonance of an asymmetric dielectric wire pair, Appl. Phys. Lett. 105 (2014) 172901, http://dx.doi.org/10.1063/1.4900757.
[15] Polina P. Vabishchevich, Sheng Liu, Michael B. Sinclair, Enhanced second-harmonic generation using broken symmetry III-V semiconductor Fano metasurfaces, ACS Photon. 5 (2018) 1685–1690, http://dx.doi.org/10.1021/acsphotonics.7b01478.
[16] Yuanlin Zheng, Jianfan Yang, Zhenhua Shen, Optically induced transparency in a micro-cavity, Light: Sci, Appl. 5 (2016) e16072, http://dx.doi.org/10.1038/lsa.2016.72.
[17] Daehan Yoo, Ferran Vidal-Codina, Cristian Ciracì, Modeling and observation of mid-infrared nonlocality in effective epsilon-near-zero ultranarrow coaxial apertures, Nature Commun. 10 (2019) 4476, http://dx.doi.org/10.1038/s41467-019-12038-3.
[18] Ashok Kodigala, Thomas Lepetit, Qing Gu, Lasing action from photonic bound states incontinuum, Nature 541 (2017) 196–199, http://dx.doi.org/10.1038/nature20799.
[19] R.F. Ndangali, S.V. Shabanov, Electromagnetic bound states in the radiation continuum for periodic double arrays of subwavelength dielectric cylinders, J. Math. Phys. 51 (2010) 102901, http://dx.doi.org/10.1063/1.3486358.
[20] C.W. Hsu, B. Zhen, J. Lee, S.-L. Chua, S.G. Johnson, J.D. Joannopoulos, M. Soljačić, Observation of trapped light within the radiation continuum, Nature 499 (2013) 188, http://dx.doi.org/10.1038/nature12289.
[21] F. Monticone, A. Alú, Embedded photonic eigenvalues in 3D nanostructures, Phys. Rev. Lett. 112 (2014) 213903, http://dx.doi.org/10.1103/PhysRevLett.112.213903.
[22] M. Rybin, Y. Kivshar, Supercavity lasing, Nature 541 (2017) 164, http://dx.doi.org/10.1038/541164a.
[23] M.A. Belyakov, M.A. Balezin, Z.F. Sadrieva, P.V. Kapitanova, E.A. Nenasheva, A.F. Sadreev, A.A. Bogdanov, Experimental observation of symmetry protected bound state in the continuum in a chain of dielectric disks, Phys. Rev. A 99 (2019) 053804, http://dx.doi.org/10.1103/PhysRevA.99.053804.
[24] Z.F. Sadrieva, I.S. Sinev, K.L. Koshelev, A. Samusev, I.V. Iorsh, O. Takayama, R. Malureanu, A.A. Bogdanov, A.V. Lavrinenko, Transition from optical bound states in the continuum to leaky resonances: role of substrate and roughness, ACS Photon. 4 (2017) 723, http://dx.doi.org/10.1021/acsphotonics.6b00860.
[25] Xu. Chen, Wenhui. Fan, Tunable bound states in the continuum in all-dielectric terahertz metasurfaces, Nanomaterials 10 (2020) 623, http://dx.doi.org/10.3390/nano10040623.
[26] S.T. Ha, Y.H. Fu, N.K. Emani, Z. Pan, R.M. Bakker, R. Paniagua-Domnguez, A.I. Kuznetsov, Directional lasing in resonant semiconductor nanoantenna arrays, Nat. Nanotechnol. 13 (2018) 1042–1047, http://dx.doi.org/10.1038/s41565-018-0245-5.
[27] Y. Plotnik, O. Peleg, F. Dreisow, M. Heinrich, S. Nolte, A. Szameit, M. Segev, Experimental observation of optical bound states in the continuum, Phys. Rev. Lett. 107 (2011) 183901, http://dx.doi.org/10.1103/PhysRevLett.107.183901.
[28] M.I. Molina, A.E. Miroshnichenko, Y.S. Kivshar, Surface bound states in the continuum, Phys. Rev. Lett. 108 (2012) 070401, http://dx.doi.org/10.1103/physrevlett.108.070401.
[29] G. Corrielli, G. Della Valle, A. Crespi, R. Osellame, S. Longhi, Observation of surface states with algebraic localization, Phys. Rev. Lett. 111 (2013) 220403, http://dx.doi.org/10.1103/PhysRevLett.111.220403.
[30] E.A. Bezus, L.L. Doskolovich, D.A. Bykov, V.A. Soifer, Spatial integration and differentiation of optical beams in a slab waveguide by a dielectric ridge supporting high-Q resonances, Opt. Express 26 (2018) 25156, http://dx.doi.org/10.1364/OE.26.025156.
[31] M.V. Rybin, K.L. Koshelev, Z.F. Sadrieva, K.B. Samusev, A.A. Bogdanov, M.F. Limonov, Y.S. Kivshar, High-Q supercavity modes in subwavelength dielectric resonators, Phys. Rev. Lett. 119 (2017) 243901, http://dx.doi.org/10.1103/PhysRevLett.119.243901.
[32] Kirill Koshelev, Sergey Lepeshov, Mingkai Liu, Andrey Bogdanov, Yuri Kivshar, Asymmetric metasurfaces with high-Q resonances governed by bound states in the continuum, Phys. Rev. Lett. 121 (2018) 193903, http://dx.doi.org/10.1103/PhysRevLett.121.193903.
[33] B. Zhen, C.W. Hsu, L. Lu, A.D. Stone, M. Soljačić, Topological nature of optical bound states in the continuum, Phys. Rev. Lett. 113 (2014) 257401, http://dx.doi.org/10.1103/PhysRevLett.113.257401.
[34] E.D. Palik, Handbook of Optical Constants of Solids, Academic, 1997.
[35] V.A. Fedotov, M. Rose, S.L. Prosvirnin, N. Papasimakis, N.I. Zheludev, Sharp trapped-mode resonances in planar metamaterials with a broken structural symmetry, Phys. Rev. Lett. 99 (2007) 147401, http://dx.doi.org/10.1103/PhysRevLett.99.147401.
[36] Rodica Moraresc, Honghui Shen, Exploiting the localized surface plasmon modes in gold triangular nanoparticles for sensing applications, J. Mater. Chem. 22 (2012) 11537–11542, http://dx.doi.org/10.1039/C2JM30944K.
[37] T. Klar, M. Perner, S. Grosse, Surface-plasmon resonances in single metallic nanoparticles, Phys. Rev. Lett. 80 (19) (1998) 4249–4252, http://dx.doi.org/10.1103/PhysRevLett.80.4249.
[38] Arash Ahmadivand, Burak Gerislioglu a, Zeinab Ramezani, Gated graphene islands enabled tunable charge transfer plasmon terahertz metamodulator, Nanoscale 11 (17) (2019) 8091–8095, http://dx.doi.org/10.1039/C8NR10151E.
[39] Burak Gerislioglu, Arash Ahmadiv, Nezih Pala, Tunable plasmonic toroidal terahertz metamodulator, Phys. Rev. B 97 (2018) http://dx.doi.org/10.1103/PhysRevB.97.161405, 161405(R).
[40] V. Nooshnab, A. Ahmadivand, Optothermally functional charge transfer plasmon modulator, IEEE Photonics Technol. Lett. 29 (18) (2017) 1556–1559, http://dx.doi.org/10.1109/LPT.2017.2736251.